International Journal of Fracture **46**: 123–140, 1990.

Micromechanics characterization of sublaminate damage

L.R. DHARANI and H. TANG
Department of Mechanical and Aerospace Engineering and Engineering Mechanics, University of Missouri-Rolla, Rolla, Missouri 65401-0249, USA

Received 15 April 1989; accepted in revised form 15 September 1989

Abstract. A micromechanics analytical model is developed for characterizing the fracture behaviour of a fibre reinforced composite laminate containing a transverse matrix crack and longitudinal debonding along 0/90 interface. Both the matrix and the fibres are considered as linear elastic. A consistent shear lag theory is used to represent the stress-displacement relations. The governing equations, a set of differential-difference equations, are solved satisfying the boundary conditions appropriate to the damage configuration by making use of an eigenvalue technique. The properties of the constituents appear in the model explicitly. Displacements and stresses in the fibres and the matrix are obtained, and the growth of damage is investigated by using the point stress criterion. The investigation includes fibre stress distribution in zero degree plies, transverse crack and debonding intitiation as functions of laminate geometry, and the effect of fibre breaks in the zero degree ply on damage growth. The predicted damage growth patterns and the corresponding critical strains agree with the finite element and experimental results.

1. Introduction

It has been generally accepted that the ultimate failure of a fibre reinforced composite laminate results when the load-carrying fibres break. However, the failure initiates at a fairly low stress level in the matrix phase of the composite when small cracks appear in the matrix. This sublaminate failure can be broadly classified into three categories: transverse cracks, free-edge delamination, and interlaminar debonding in the direction of load carrying fibres (longitudinal cracks). These three sublaminate failure modes are depicted in Fig. 1.

In particular, matrix transverse cracks appear at a much lower stress than those predicted by classical lamination theory and first ply failure criterion. Garrett and Bailey [1], Parvizi and Bailey [2] and Parvizi et al. [3] described and explained the occurrence of systematic transverse cracking at low strains of the inner ply in three layered glass fibre polyester and epoxy cross ply laminates in which a tensile load was applied parallel to the fibres in the outer plies. Reifsnider and others [4, 5] conducted a number of experimental investigations on composite laminates and established the dependence of stiffness and fatigue life of a composite laminate on transverse cracking. Crossman and Wang [6, 7], Crossman et al. [8] and Wang et al. [9] demonstrated that stress analysis, which is based on the laminated plate theory, is inadequate for predicting transverse cracking and the initiation of delamination. They predicted transverse cracking and edge delamination by using a generalized plane strain, finite-element analysis to calculate the strain energy release rates. The investigators above have reported the presence of longitudinal cracking parallel to load carrying fibres and the coupling between transverse cracks and longitudinal cracks.

This paper deals with the development of a micromechanics analytical shear lag model for predicting the onset and growth of longitudinal crack at the tip of an existing transverse

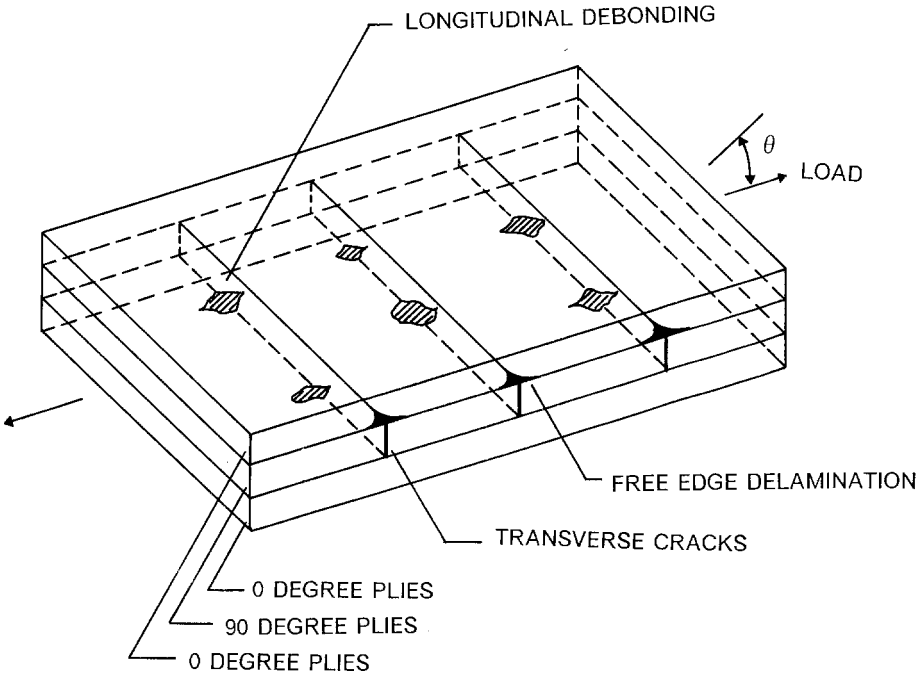

Fig. 1. Schematic view of sub-laminate damage pattern.

crack in a laminate. The model is based on a consistent shear lag theory developed recently by Sendeckyj and Jones [10, 11] which unlike the classical shear lag models [12, 13] predicts fibre as well as matrix stresses accurately. The governing equations are solved using an efficient eigenvalue solution technique [14], rather than a Fourier transform technique used in most of the earlier shear lag models [10–13]. The self-similar growth of an initial inherent transverse crack through the transverse plies is predicted based on the point stress criterion; failure occurs when the axial stess in the unbroken ligament at the crack tip reaches the ultimate tensile strength of the matrix or the fibre depending on the ligament location. The onset of delamination along the interface between the axial plies and transverse plies is assumed to occur when the interfacial shear stress reaches the matrix shear strength. The model predictions are compared with those of finite element and experimental results.

2. Formulation

A schematic edge view typical of a laminate considered in the analysis is shown in Fig. 2. It consists of angle plies, zero degree plies, and 90 degree plies; zero degree direction coincides with the load axis. A single transverse crack lies entirely in the 90 degree plies. It is further assumed that the transverse crack lies in the matrix phase with no fibre splits. At either end of the transverse crack, longitudinal cracks of arbitrary length (β) are located. The load carrying plies may contain an arbitrary number of broken fibres; fibre breaks in these plies may or may not form a continuous transverse notch. The laminate is then subjected to a remote uniform tensile strain. The elements marked A, B and C in Fig, 2 are represented

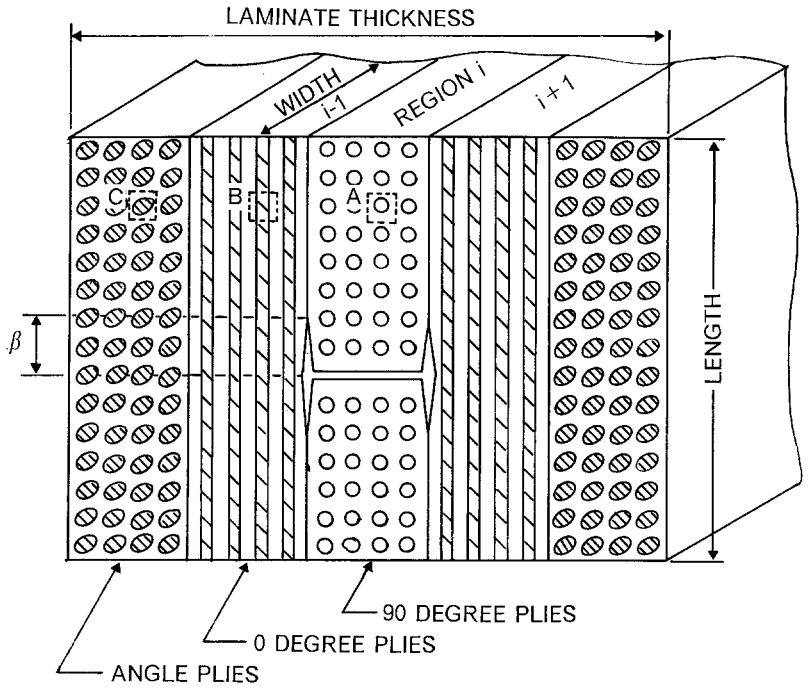

Fig. 2. Idealized sublaminate damage model-end view.

by equivalent unidirectional fibre-matrix elements such that the longitudinal and transverse moduli of the equivalent elements are the same as those of the corresponding actual elements. With this idealization the edge view shown in Fig. 2 can be schematically represented as a combination of five two-dimensional unidirectional regions, each region having different equivalent fibres as shown in Fig. 3. The transverse crack is formed by breaking equivalent fibes in the region of 90-degree plies. The longitudinal symmetric debonding is assumed at the crack tips. After having established a unidirectional region consisting of parallel fibres in the direction of the applied load a generalized consistent shear lag theory is developed in the following section.

2.1. Generalized consistent shear-lag model

Let us consider a unidirectional region shown in Fig. 3, with or without damage, subjected to some forces or constrained displacements at infinity and free of stresses on both sides. A typical fibre/matrix element from the lamina such as element A in Fig. 3 which is of finite width h and an infinitesimal height dy is considered for the analysis. The properties of the fibre and the matrix for each element may be different. For the sake of simplicity, during derivation, the heterogeneous fibre/matrix element is replaced by an equivalent homogeneous orthotropic element [10, 11] in which the properties of the fibre and the matrix are smeared out through the use of micromechanics [15]. This homogeneous element is shown in Fig. 4 along with various stress components. With reference to the free body diagram shown in Fig. 4 the equilibrium equations in the transverse (x) and axial (y) directions for a generic element n and special element at the free edge ($n = 1$ and $n = N$)

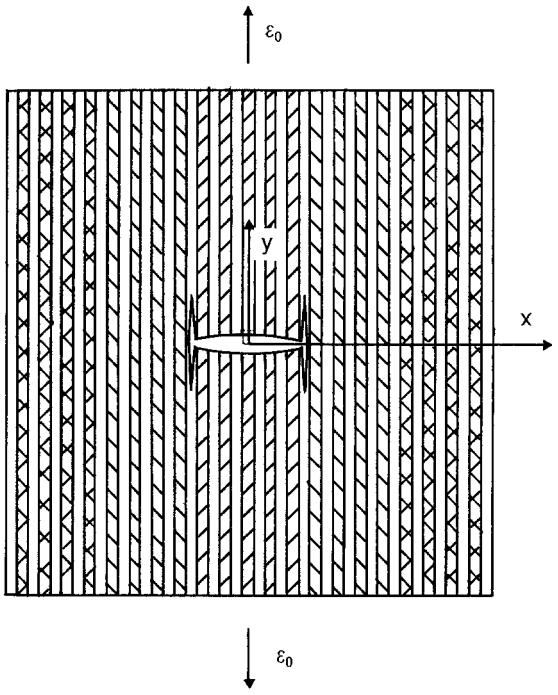

Fig. 3. Equivalent unidirectional region.

can be written as

$$\sigma_{x(n+1/2)} - \sigma_{x(n-1/2)} + \frac{h}{2}\left[\tau_{(n+1/2)y} + \tau_{(n-1/2)y}\right] + \delta_{n1}\left[\sigma_{x(n-1/2)} - \frac{h}{2}\tau_{(n-1/2)y}\right]$$

$$+ \delta_{nN}\left[-\sigma_{x(n+1/2)} - \frac{h}{2}\tau_{(n+1/2)y}\right] = 0, \tag{1a}$$

$$\tau_{(n+1/2)} - \tau_{(n-1/2)} + h\sigma_{yn,y} + \delta_{n1}\tau_{(n-1/2)} - \delta_{nN}\tau_{(n+1/2)} = 0 \quad n = 1, 2, \ldots, N, \tag{1b}$$

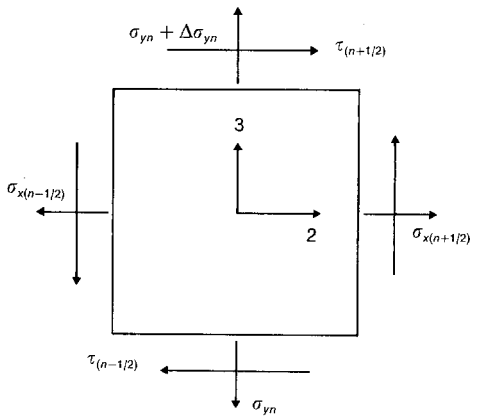

Fig. 4. Free body diagram of homogeneous element.

where the subscripts $(n + 1/2)$ and $(n - 1/2)$ indicate the mid-nodes between the elements n and $(n + 1)$ and $(n - 1)$ and n respectively, subscript y preceded by a comma indicates differentiation with respect to y, and δ_{nm} is Kronecker delta ($\delta_{nm} = 0$ for $m \neq n$ and $\delta_{nm} = 1$ for $m = n$).

Next, a set of approximate constitutive relations are derived. In general, the constitutive equations for a homogeneous, orthotropic material can be written as [15]

$$\sigma_x = C_{11}u_{,x} + C_{12}v_{,y}, \tag{2a}$$

$$\sigma_y = C_{12}u_{,x} + C_{22}v_{,y}, \tag{2b}$$

$$\tau = C_{66}(u_{,y} + v_{,x}), \tag{2c}$$

where u and v are the x and y components of the displacements, C_{ij} are the orthotropic elastic constants. These general relations can be applied to any element n by replacing C_{ij} in (2) with the constants C_{ij}^n appropriate to that element. The elastic constants for an element can be expressed in terms of fibre and matrix properties as

$$C_{22}^n = \gamma C_{22f}^n + (1 - \gamma)C_{22m}^n, \quad C_{11}^n = C_{11f}^n C_{11m}^n/[\gamma C_{11m}^n + (1 - \gamma)C_{11f}^n],$$

$$C_{12}^n = \gamma C_{12f}^n + (1 - \gamma)C_{12m}^n, \quad C_{66}^n = C_{66f}^n C_{66m}^n/[\gamma C_{66m}^n + (1 - \gamma)C_{66f}^n], \tag{3}$$

where subscripts f and m represent the fibre and the matrix respectively and $\gamma = b/h$. The mid-node $(n + 1/2)$ is common to elements n and $(n + 1)$. The transverse stress, $\sigma_{x(n+1/2)}$, at mid-node is interpreted as

$$\sigma_{x(n+1/2)} = \tfrac{1}{2}[\sigma_{x(n+1/2)}|^- + \sigma_{x(n+1/2)}|^+], \tag{4}$$

where $\sigma_{x(n+1/2)}|^-$ is the mid-node stress from left and $\sigma_{x(n+1/2)}|^+$ is the corresponding stress from right. The mid-node shear stress is interpreted likewise. Following (2), we can write

$$\sigma_{x(n+1/2)} = \tfrac{1}{2}\{[C_{11}^n u_{(n+1/2),x} + C_{12}^n v_{(n+1/2),y}]^- + [C_{11}^{n+1} u_{(n+1/2,x} + C_{12}^{n+1} v_{(n+1/2),y}]^+\}, \tag{5a}$$

$$\sigma_{ym} = C_{12}^n u_{n,x} + C_{22}^n v_{n,y}, \tag{5b}$$

$$\tau_{(n+1/2)} = \tfrac{1}{2}\{C_{66}^n[u_{(n+1/2),y} + v_{(n+1/2),x}]^- + C_{66}^{n+1}[u_{(n+1/2),y} + v_{(n+1/2),x}]^+\}. \tag{5c}$$

To make the problem mathematically tractable, the differentials with respect to x are approxmated by (central, backward and forward) difference formulas. Further, the mid-node displacements are approximated by the average of the centre line displacements of the adjoining elements. These approximations are

$$u_{n,x} = \frac{1}{h}[u_{(n+1/2)} - u_{(n-1/2)}], \tag{6a}$$

$$u_{(n+1/2),x}|^- = \frac{2}{h}[u_{(n+1/2)} - u_n], \tag{6b}$$

$$u_{(n+1/2),x}|^{+} = \frac{2}{h}[u_{(n+1)} - u_{(n+1/2)}], \tag{6c}$$

$$u_{(n+1/2)} = \tfrac{1}{2}[u_n + u_{(n+1)}], \tag{6d}$$

$$v_{(n+1/2)} = \tfrac{1}{2}[v_n + v_{(n+1)}]. \tag{6e}$$

With these approximations the constitutive relations for element n can be written as

$$\sigma_{x(n+1/2)} = \frac{1}{2h}(C_{11}^{n} + C_{11}^{n+1})(u_{n+1} - u_n) + \tfrac{1}{2}(C_{12}^{n} + C_{12}^{n+1})v_{n+1/2,y}, \tag{7a}$$

$$\sigma_{y(n)} = C_{12}^{n}(u_{n+1/2} - u_{n-1/2})/h + C_{22}^{n}v_{n,y}, \tag{7b}$$

$$\tau_{n+1/2} = \tfrac{1}{2}(C_{66}^{n} + C_{66}^{n+1})u_{n+(1/2),y} + (v_{n+1} - v_n)/h]. \tag{7c}$$

The transverse and shear stresses at $(n - 1/2)$ can be obtained by substituting $(n - 1)$ for n in (7a, 7c).

Substituting (7) into (1) the equilibrium equations in terms of the displacements can be obtained. These equations can be converted into a more convenient dimensionless form by making a change in the variable, $y = h\eta$. With some further simplifications the final equilibrium equations are obtained and written in the following matrix form:

$$\frac{\mathrm{d}^2\{u\}}{\mathrm{d}\eta^2} - [K_u]\{u\} = [C_u]\frac{\mathrm{d}\{v\}}{\mathrm{d}\eta} \tag{8a}$$

and

$$\frac{\mathrm{d}^2\{v\}}{\mathrm{d}\eta^2} - [K_v]\{v\} = [C_v]\frac{\mathrm{d}\{u\}}{\mathrm{d}\eta}, \tag{8b}$$

where, vector $\{u\}$ and $\{v\}$ are

$$\{u\} = \{u_1, u_2, \ldots, u_N\},$$

$$\{v\} = \{v_1, v_2, \ldots, v_N\},$$

with u_n and v_n representing the x and y displacement components of fibre n and the tridiagonal matrices $[K_u]$, $[K_v]$, $[C_u]$, and $[C_v]$ are given in Appendix A. Equations (8a, 8b) can be reduced to a first order equation

$$\frac{\mathrm{d}\{w\}}{\mathrm{d}\eta} = [K_w]\{w\}, \tag{9}$$

where

$$\{w\} = \left\{u_1, \ldots, u_N, v_1, \ldots, v_N, \frac{du_1}{d\eta}, \ldots, \frac{du_N}{d\eta}, \frac{dv_1}{d\eta}, \ldots, \frac{dv_N}{d\eta}\right\}^T,$$

$$[K_w] = \begin{bmatrix} 0 & 0 & [1] & 0 \\ 0 & 0 & 0 & [1] \\ [K_u] & 0 & 0 & [C_u] \\ 0 & [K_v] & [C_v] & 0 \end{bmatrix}_{4N \times 4N}$$

The general solution of the above equations can be written down if the eigenvalues and eigenvectors of matrix $[K_w]$ are known. Let $r_j, j = 1, 2, \ldots, K_1$ be the real eigenvalues of the matrix $[K_w]$, $\{A_j\}, \{B_j\}$ be the first $2N$ components of the corresponding eigenvectors, and $p_j + iq_j$, p_j, $q_j > 0$, $j = 1, 2, \ldots, K_2$ be the complex eigenvalues of the matrix $[K_w]$. $\{A_j^R\} + i\{A_j^I\}, \{B_j^R\} + i\{B_j^I\}$ be the first $2N$ components of the corresponding eigenvectors, K_1 and K_2 are the number of the real and complex eigenvalues respectively, so that, $K_1 + 2K_2 = 4N$. The eigenvalues can be readily calculated numerically once the matrix $[K_w]$ is formed. Then, the general solution to (9) is

$$\{u\} = \sum_{j=1}^{K_1} C_j(A_j)e^{r_j\eta} + \sum_{j=1}^{K_2} e^{p_j\eta}[C_j^1(\{A_j^R\} \cos q_j\eta - \{A_j^I\} \sin q_j\eta) + C_j^2(\{A_j^R\} \sin q_j\eta + \{A_j^I\} \cos q_j\eta)], \tag{10a}$$

$$\{v\} = \sum_{j=1}^{K_1} C_j(B_j\}e^{r_j\eta} + \sum_{j=1}^{K_2} e^{p_j\eta}[C_j^1(\{B_j^R\} \cos q_j\eta - \{B_j^I\} \sin q_j\eta) + C_j^2(\{B_j^R\} \sin q_j\eta + \{B_j^I\} \cos q_j\eta)], \tag{10b}$$

where C_j, C_j^1, C_j^2 are the $4N$ constants to be determined from the boundary conditions. In the following sections the appropriate boundary conditions for the two damage configurations, transverse cracking only and transverse cracking with longitudinal splitting, are discussed.

2.2. Transverse cracking

A transverse crack is formed by breaking the "equivalent fibres" in the 90 degree plies. The appropriate boundary conditions are

$$\{\varepsilon_y\}|_{\eta=\eta_s} = \varepsilon_0, \tag{11a}$$

$$\{\tau\}|_{\eta=\eta_s} = \{\tau\}|_{\eta=0} = 0, \tag{11b}$$

$$[T_5]\{v\}|_{\eta=0} + [T_6]\{\sigma_y\}|_{\eta=0} = 0, \tag{11c}$$

where $[T_6]$ is a diagonal matrix with non-zero elements of unit magnitude from $N1$ to $N2$ only and $[T_5] = [I] - [T_6]$ with $[I]$ being a unit matrix.

By substituting (7) and (10) into the above boundary conditions equations (11) we get a system of linear algebraic equations for the unknown constants C_j, C_j^1, and C_j^2. Once these constants are known the displacements and stresses at any location can be calculated.

2.3. Transverse cracking and longitudinal delamination

To apply the generalized consistent shear-lag solutions to the problem of transverse cracking with longitudinal delamination the unidirectional region is divided into four regions as shown in Fig. 5. The necessary boundary conditons for various regions are

$$v_n|_{\eta=0} = \tau_n|_{\eta=0} = 0 \quad \text{for regions 2 and 3,} \tag{12a}$$

$$\sigma_{yn}|_{\eta=0} = \tau_n|_{\eta=0} = 0 \quad \text{for region 1,} \tag{12b}$$

$$\varepsilon_{yn}|_{\eta\to+\infty} = \varepsilon_0, \quad \tau_n|_{\eta\to+\infty} = 0 \quad \text{for region 4.} \tag{12c}$$

In addition to the above boundary conditions the axial displacement v_n, the transverse displacement u_n, the axial stress σ_{yn}, and the transverse stress σ_{xn} of a fibre n must be continuous along $\eta = \eta_s$.

Because region 4 is an infinite strip, the expressions for displacements $\{u\}$ and $\{v\}$ will be different from those given by (10), which correspond to regions of finite length. Since the strains (therefore stresses) should remain finite when $\eta \to +\infty$, those terms with positive eigenvalues in the displacements, (10), must be zero. From this it can be seen that the matrix $[K_w]$ has a zero eigenvalue with two independent eigenvectors $\{1, \ldots, 1, 1, \ldots, 1, 0, \ldots, 0, 0, \ldots, 0\}$ and $\{1, \ldots, 1, -1, \ldots, -1, 0, \ldots, 0, 0, \ldots, 0\}$. The displacements for the

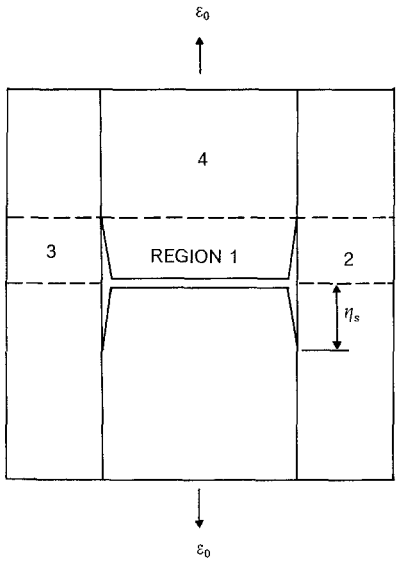

Fig. 5. Transverse crack with splitting.

region 4 are

$$\{u\} = (C_0 - \varepsilon_0\eta)\{1\} + \sum_{j=1}^{K_1} C_j\{A_j\}e^{-r_j\eta} + \sum_{j=1}^{K_2} e^{-p_j\eta}[C_j^1(\{A_j^R\}\cos q_j\eta - \{A_j^I\}\sin q_j\eta) + C_j^2(\{A_j^R\}\sin q_j\eta + \{A_j^I\}\cos q_j\eta)], \quad (13a)$$

$$\{v\} = (C_0 + \varepsilon_0\eta)\{1\} + \sum_{j=1}^{K_1} C_j\{B_j\}e^{-r_j\eta} + \sum_{j=1}^{K_2} e^{-p_j\eta}[C_j^1(\{B_j^R\}\cos q_j\eta - \{B_j^I\}\sin q_j\eta) + C_j^2(\{B_j^R\}\sin q_j\eta + \{B_j^I\}\cos q_j\eta)]. \quad (13b)$$

Clearly the boundary conditions equations (12) have been satisfied.

By applying (10) to regions 1, 2 and 3 separately and satisfying the boundary conditions and continuity conditions, a system of linear algebraic equations for the unknown constants corresponding to each region are obtained. After solving these equations, the stresses and strains in any fibre/matrix element can be obtained.

2.4. Numerical solution scheme

One of the major advantages of the present model is that simple explict expressions for the displacements and stresses have been obtained. In each case it is a linear combination of a finite number of functions of the form $e^{\zeta x}$. Clearly, the bigger the number N is, the more accurate the calculation of the displacements will be. However, due to the limitation on computer capacity and numerical errors, there is a limit on that number N over which no practical benefit could be derived. As shown in Fig. 3 each element consists of one fibre surrounded by the matrix on either side. Thus it seems that the number N would be the total number of fibres in the entire region. However, since the equivalent homogeneous element has been adapted during derivation, we can construct the element as a combination of two or more fibres or divide one layer into more than one element. Thus the number N can always be kept around an optimum value.

3. Results and discussion

3.1. Analytical results

The results are given for a laminate with an idealized cracking geometry shown in Fig. 2. It is assumed that the crack growth path is one dimensional and the crack front is represented by a point. Symmetric graphite/epoxy laminates of $[0_m/90_n]_s$ and $[\theta_k/0_m/90_n]_s$ types are considered in the analysis. The following properties along the material principal axes are used in the calculations: $E_1 = 144.8\,\text{GPa}$, $E_2 = E_3 = 11.7\,\text{GPa}$, $G_{12} = G_{13} = 6.5\,\text{GPa}$, $G_{23} = 3.5\,\text{GPa}$, $\mu_{12} = \mu_{13} = 0.3$, $\mu_{23} = 0.54$, matrix tensile strength $= 80\,\text{MPa}$, and matrix shear strength 40 MPa where axis 1 is aligned in the fibre direction and plane 2–3 is normal to it.

First, the self-similar growth of an initial (inherent) transverse crack through the 90 degree plies is presented based on the point stress criterion; failure occurs when the stress in the unbroken element reaches the ultimate stress of the fibre or the matrix depending on the element location. Since the region of 90 degree plies has been replaced by equivalent 0 degree plies the ultimate stress of this equivalent fibre is assumed to be approximately equal to that of the neat matrix material. The inherent flaw size is approximately 2.6 T to 3.6 T [9] where T is the ply thickness. Second, the onset of delamination along the 0/90 interface parallel to the applied load and the extension of the transverse crack into the 0 degree plies by breaking axial fibres is investigated. The delamination is assumed to occur when the interfacial shear stress reaches the matrix shear strength. The point stress criterion was proposed by Nuismer and Whitney [16] for notched composites. This criterion has been extended to shear lag models for unidirectional composites [13, 17] with some success. To illustrate the application of the failure criterion, let us consider a transverse crack contained in 90 degree plies of $[0_2/90_2]$, symmetric laminate. For a normalized crack length of 0.4 and an applied remote strain of 0.45 percent the analytical model would predict an axial stress of 80 MPa and a shear stress of 21 MPa in the matrix ligament at the crack tip. If the ultimate tensile and shear strengths of the matrix are 80 MPa and 40 MPa, respectively, the point stress criterion would predict a self-similar cracking.

Figures 6 and 7 show the remote strain required to extend an inherent transverse crack, as a function of the 90 degree layer thickness for $[0_m/90_n]_s$ and $[45_k/0_m/90_n]_s$ laminates respectively. The tendency of the laminate for microcracking in the transverse plies increases with the transverse ply thickness. The axial plies provide substantial constraint for smaller 90 degree ply thicknesses. For a given 90 degree ply thickness the addition of zero degree plies increases the transverse cracking strain. A comparison of Fig. 6 and Fig. 7 shows that the presence of angle plies decreases the transverse cracking strain for smaller 90 degree layer thicknesses.

The tendency of laminates to delaminate along the 0/90 interface in the presence of a transverse crack is studied next. Figures 8 and 9 show the laminate strain at the onset of delamination (splitting) along the 0/90 interface for the $[0_m/90_n]_s$ and $[\theta_2/0_m/90_n]_s$ laminates for various 90 degree ply thicknesses. Here, it is assumed that a transverse crack has already

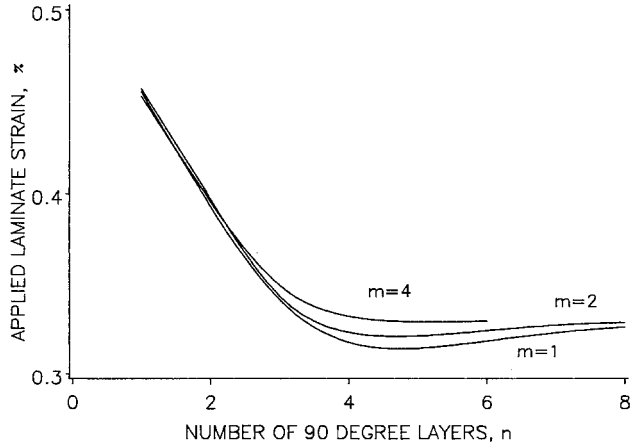

Fig. 6. Predicted tensile strain at the onset of transverse cracking for $[0_m/90_n]_s$ laminates.

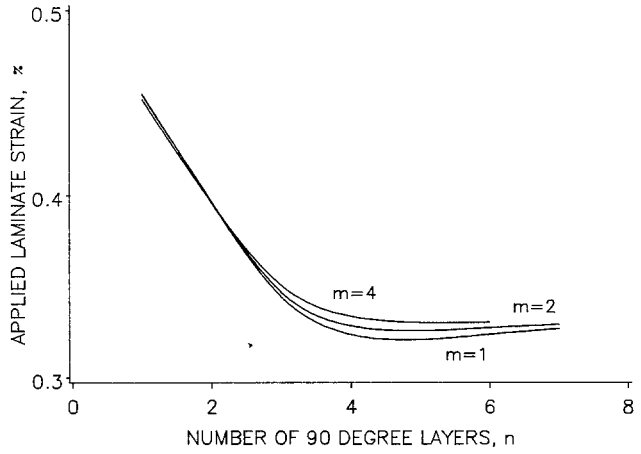

Fig. 7. Predicted tensile strain at the onset of transverse cracking for $[45_2/0_m/90_n]_s$ laminates.

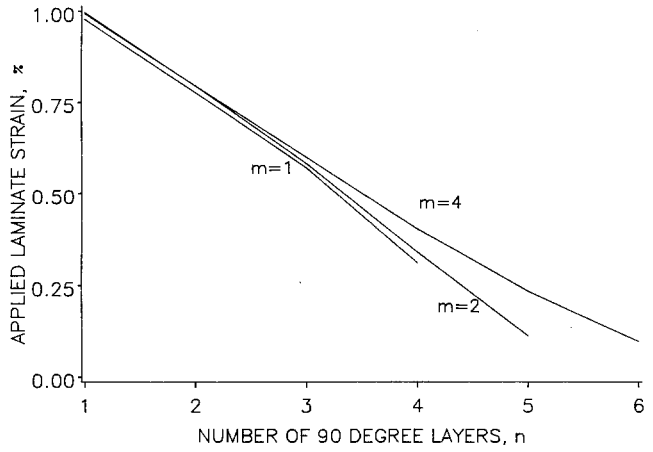

Fig. 8. Predicted tensile strain at the onset of delamination for $[0_m/90_n]_s$ laminates.

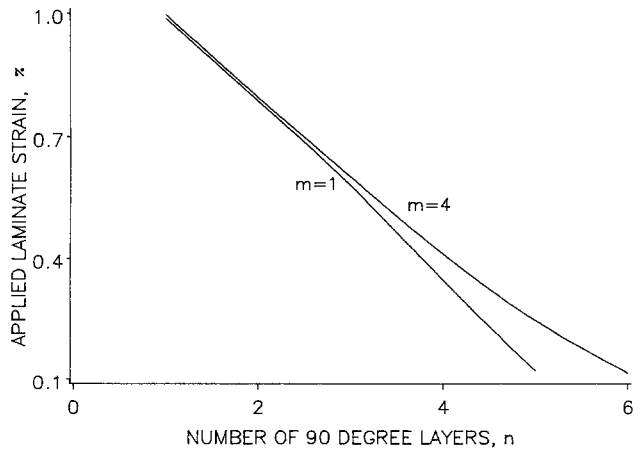

Fig. 9. Predicted tensile strain at the onset of delamination for $[45_2/0_m/90_n]_s$ laminates.

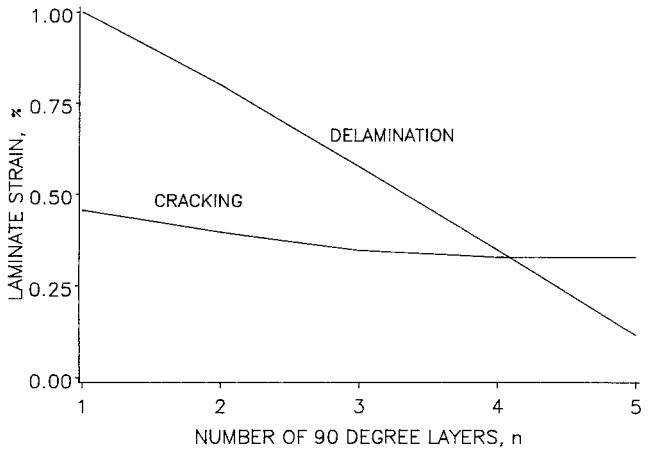

Fig. 10. Laminate strain for the onset of transverse cracking or delamination at the interface.

propagated up to the interface and that the interface delamination occurs due to the large shear stress at the transverse crack tip. For the two types of laminates it can be seen that the tendency for delamination increases with an increase in 90 degree layer thickness. In Fig. 10 the laminate strains for the onset of interface delamination are compared with those for the onset of transverse cracking for a $[0_2/90_n]_s$ laminate. For thinner 90 degree layers the delamination strain is much higher than the transverse cracking strain and hence the laminates with a few 90 degree plies would exhibit only transverse cracking. However, the laminates with thicker 90 degree layer would delaminate following a transverse cracking.

Next, the crack tip stress and strain distributions along with maximum stresses are presented. Of particular interest is the role of the crack tip stress field on the failure modes, such as self-similar cracking in the 90 degree layer as well as in the 0 degree layer, matrix splitting in the 90 degree layer and the 0/90 interface delamination. The crack tip axial strain distribution for a unit applied laminate strain is shown in Fig. 11 for various crack lengths. As the crack propagates toward the 0/90 interface the maximum (crack tip) strain increases until the tip is very close to the interface and then begins to decrease. When the crack tip is

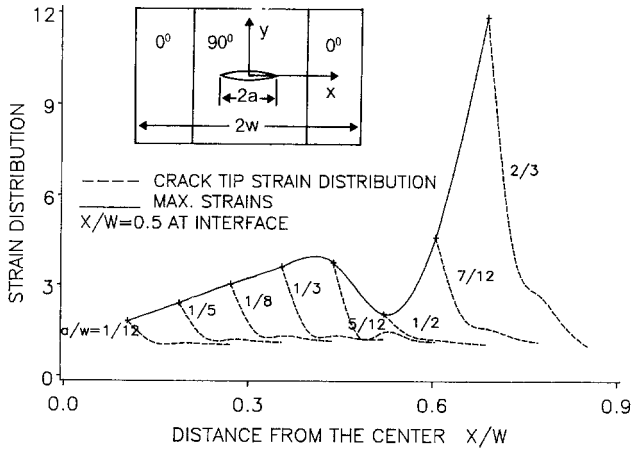

Fig. 11. Crack tip strain distributions and maximum strains.

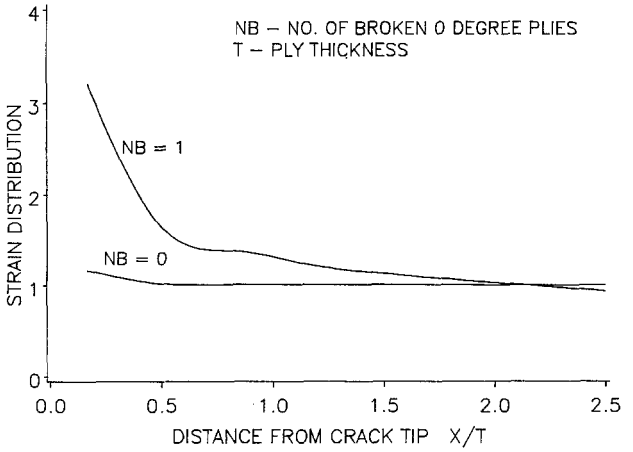

Fig. 12. Strain distribution in zero degree plies for $[0_2/90]_s$ laminates.

at the 0/90 interface the crack tip maximum axial strain (now in the first 0 degree ply) is significantly smaller. However, once a 0 degree ply breaks then the maximum strain increases with the crack length, indicating an unstable crack growth in the 0 degree layer once it is initiated in it. This is further illustrated in Fig. 12 in which two crack tip strain distributions in the 0 degree layer are plotted, one with no broken plies in the 0 degree layer and the other with a single broken 0 degree ply.

The possibility of a longitudinal matrix splitting within the 90 degree layer is also studied. In Fig. 13, applied laminate strain required for the self-similar growth of an existing transverse flaw and that required for the longitudinal matrix splitting respectively are shown for various crack lengths for $[0_2/90_2]_s$ laminate. For the most part the strain for splitting is much higher than that required for self-similar crack extension. When the crack has extended through the entire thickness of the 90 degree layer the situation is reversed. Therefore, it can be observed that a transverse (inherent) flaw generally grows in a self-similar fashion up to the 0/90 interface and then only interface delamination may occur.

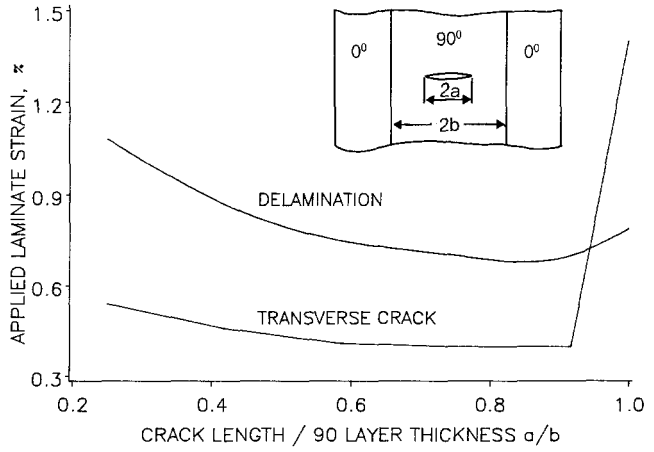

Fig. 13. Failure modes.

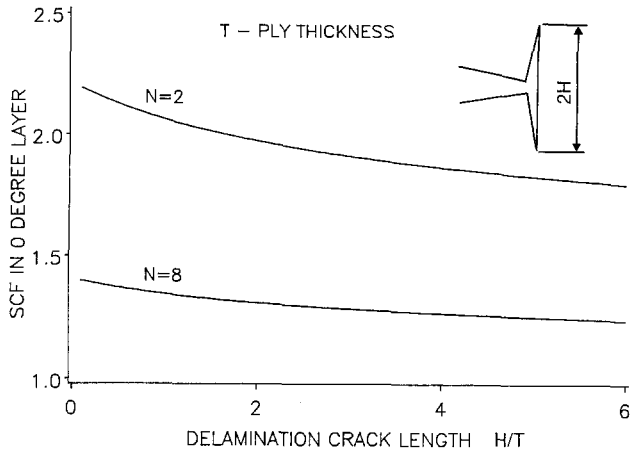

Fig. 14. Effect of delamination on maximum axial strain for $[0_2/90]_s$ laminates.

Finally, the effect of 0/90 interface delamination crack on the fibre and matrix stresses is presented. In Fig. 14 the maximum axial strain in the first 0 degree ply along the transverse crack plane (x-axis) is plotted for two laminates. As the delamination grows the maximum strain in the 0 degree ply decreases, indicating that once the 0/90 interface fails the transverse crack extension into 0 degree plies would not occur. The shear and transverse normal stresses in the matrix at the top of the interface delamination crack are presented in Fig. 15 for various delamination crack lengths for the two laminates. The transverse normal stress σ_x increases with the crack length initially and then drops, whereas the shear stress τ increases monotonically. Therefore, if the delamination were to initiate due to transverse normal stress then it would be arrested. On the other hand, if the delamination were to initiate due to shear stress then it would propagate in an unstable manner. Also plotted in Fig, 15 is the principal shear stress neglecting the axial stress in the matrix. A failure criterion based on the principal shear stress would predict unstable and stable crack growth regions.

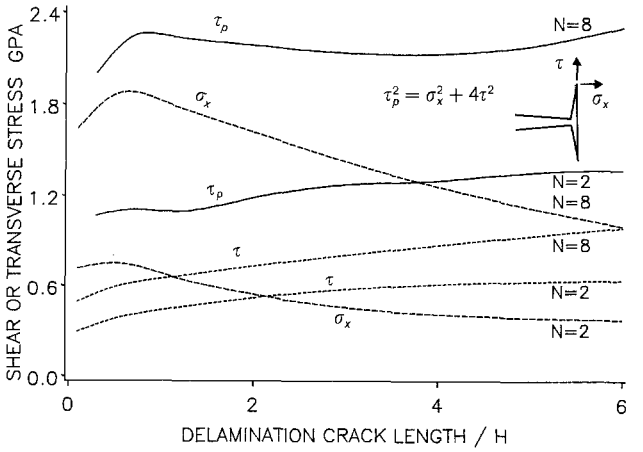

Fig. 15. Crack tip stress distributions for $[0_2/90]_s$ laminates.

Table 1. Summary of predicted and experimental results

Laminate type	Laminate tensile strain at onset of transverse cracking		
	Experimental [9]	Predicted (present model)	Predicted [9]
$[0_2/90]_s$	0.55% to 0.57%	0.46%	0.59%
$[0_2/90_2]_s$	0.29% to 0.36%	0.40%	0.36%
$[0_2/90_4]_s$	0.24% to 0.28%	0.32%	0.27%
$[0_2/90_8]_s$	0.19%	0.28%	–

Table 2. Summary of predicted and experimental results

Laminate type	Laminate tensile strain at onset of interface delamination		
	Experimental [9]	Predicted (present model)	Predicted [9]
$[0_2/90]_s$	(not observed)	1.12%	1.2%
$[0_2/90_2]_s$	0.92%	0.81%	1.05%
$[0_2/90_4]_s$	< 0.8%	0.35%	0.78%

3.2. Comparison with experimental results

Using the material properties listed in Table 1, which approximately correspond to a graphite/epoxy (T300/934) unidirectional lamina, the predicted laminate strains for transverse cracking as well as interface delamination in various laminates are compared with finite element predictions and experimental results [9]. These are summarized in Table 1 for transverse cracking and in Table 2 for interface delamination. The predictions of the current model do not include thermal (residual) stresses. The agreement between the results with respect to the transverse cracking event is good. With respect to the delamination event the agreement is good considering the fact that the experimental data is limited. Inclusion of thermal effects should substantially improve the predictions.

3.3. Some comments on element size

For a continuous medium the elastic stress field at the crack tip is unbounded. The finite difference solution, however, provides only an averaged stress state in each finite-difference element near the crack tip. Thus, the crack tip stress in the current discretized model like all shear lag models is finite. Further, the calculated element stresses depend on the element size. In the present work the size of the finite-difference element is the same as the fibre-matrix element size. This selection of the element size implies that the variation of stresses is averaged over one fibre centre-line spacing. Most discretized composite models such as those based on shear lag assumptions treat the stresses in a shear lag element to be constant and get good results for fibre-dominant composites.

4. Conclusions

The material properties appear explicitly in the model. The model can account for the self-similar growth of inherent flaws in the transverse plies, fibre fracture in the load carrying

axial plies and interface delamination between zero and 90 degree plies. The applied load is tensile in nature and is parallel to axial plies. Based on a simple point stress criterion (tensile or shear) the three failure modes, transverse crack growth in the 90 degree plies, fibre breaks in the axial plies and interface delamination, are predicted from the constituent properties and the laminate configuration. The focus of this research has been in studying the onset and growth of delamination at the 0/90 interface when the transverse crack intersects the interface. The predictions agree with the experimental as well as finite element results.

Appendix A

The matrix $[K_u]$ appearing in (7) is

$$\begin{bmatrix} (K_u)_{1,1}(K_u)_{1,2} & & & & & & \\ \cdots & & & & & & \\ & \cdots & & & & & \\ & & \cdots & & & & \\ & & & (K_u)_{n,n-1}(K_u)_{n,n}(K_u)_{n,n+1} & & & \\ & & & \cdots & & & \\ & & & & \cdots & & \\ & & & & & \cdots & \\ & & & & & & (K_u)_{N-1,N}(K_u)_{N,N} \end{bmatrix} \tag{A1}$$

with the non-zero elements $(K_u)_{i,j}$ given by

$$\begin{aligned} (K_u)_{1,1} &= -(K_u)_{1,2} = 2\frac{C_{12}^{1\frac{1}{2}}}{C_{66}^{1}}, \qquad (K_u)_{n,n-1} = -\frac{C_{11}^{n-\frac{1}{2}}}{C_{66}^{n}}, \\ (K_u)_{n,n} &= \frac{C_{11}^{n-1} + 2C_{11}^{n} + C_{11}^{n+1}}{2C_{66}^{n}}, \quad (K_u)_{n,n+1} = -\frac{C_{11}^{n+\frac{1}{2}}}{C_{66}^{n}}, \\ (K_u)_{N,N-1} &= -(K_u)_{N,N} = -2\frac{C_{11}^{N-\frac{1}{2}}}{C_{66}^{N}}. \end{aligned} \tag{A2}$$

The matrices $[K_v]$, $[C_u]$, and $[C_v]$ are also tridiagonal matrics with their non-zero elements given respectively by

$$\begin{aligned} (K_v)_{1,1} &= -(K_v)_{1,2} = \frac{C_{66}^{1\frac{1}{2}}}{C_{22}^{1}}, \quad (K_v)_{n,n-1} = -\frac{C_{66}^{n-\frac{1}{2}}}{C_{22}^{n}}, \\ (K_v)_{n,n} &= \frac{C_{66}^{n-\frac{1}{2}} + C_{66}^{n+\frac{1}{2}}}{C_{22}^{n}}, \qquad (K_v)_{n,n+1} = -\frac{C_{66}^{n+\frac{1}{2}}}{C_{22}^{n}}, \\ (K_v)_{N,N-1} &= -(K_v)_{N,N} = -C_{66}^{N-\frac{1}{2}}, \end{aligned} \tag{A3}$$

$$
\begin{aligned}
(C_u)_{1,1} &= \frac{C_{66}^{1\frac{1}{2}} - C_{12}^{1\frac{1}{2}}}{C_{66}^{1}}, & (C_u)_{1,2} &= \frac{-C_{66}^{1\frac{1}{2}} - C_{12}^{1\frac{1}{2}}}{C_{66}^{1}}, \\
(C_u)_{n,n-1} &= \frac{C_{12}^{n-\frac{1}{2}} + C_{66}^{n-\frac{1}{2}}}{2C_{66}^{n}}, & (C_u)_{n,n} &= -\frac{C_{12}^{n+1} - C_{12}^{n-1} + C_{66}^{n+1} - C_{66}^{n-1}}{4C_{66}^{n}}, \\
(C_u)_{n,n+1} &= -\frac{C_{12}^{n+\frac{1}{2}} + C_{66}^{n+\frac{1}{2}}}{2C_{66}^{n}}, & (C_u)_{N,N-1} &= \frac{C_{66}^{N-\frac{1}{2}} + C_{12}^{N-\frac{1}{2}}}{C_{66}^{N}}, \\
(C_u)_{N,N} &= \frac{C_{12}^{N-\frac{1}{2}} - C_{66}^{N-\frac{1}{2}}}{C_{66}^{N}},
\end{aligned}
\tag{A4}
$$

$$
\begin{aligned}
(C_v)_{1,1} &= \frac{C_{12}^{1} - C_{66}^{1\frac{1}{2}}}{2C_{22}^{1}}, & (C_v)_{1,2} &= \frac{-C_{12}^{1} - C_{66}^{1\frac{1}{2}}}{2C_{22}^{1}}, \\
(C_v)_{n,n-1} &= \frac{C_{12}^{n} + C_{66}^{n-\frac{1}{2}}}{2C_{22}^{n}}, & (C_v)_{n,n} &= \frac{C_{66}^{n-1} - C_{66}^{n+1}}{2C_{22}^{n}}, \\
(C_v)_{n,n+1} &= -\frac{C_{12}^{n} + C_{66}^{n+\frac{1}{2}}}{2C_{22}^{n}}, & (C_v)_{N,N-1} &= \frac{C_{12}^{N} + C_{66}^{N-\frac{1}{2}}}{2C_{22}^{N}}, \\
(C_v)_{N,N} &= \frac{C_{66}^{N-\frac{1}{2}} - C_{12}^{N}}{2C_{66}^{N}}.
\end{aligned}
\tag{A5}
$$

Acknowledgement

This work was supported by Grant NSF MSM8504591 from the National Science Foundation. The first author gratefully acknowledges the valuable discussions he had with Professor A.S.D. Wang, Drexel University, and Dr. N.J. Pagano, Air Force Material Laboratory, on constrained cracking and Dr. W.F. Jones, Oak Ridge National Laboratory, and Dr. G.P. Sendeckyj, Air Force Flight Dynamics Laboratory, on consistent shear lag theory.

References

1. K.W. Garrett and J.E. Bailey, *Journal of Materials Science* 12 (1977) 157.
2. A. Parvizi and J.E. Bailey, *Journal of Materials Science* 13 (1978) 2131.
3. A. Parvizi, K.W. Garrett and J.E. Bailey, *Journal of Materials Science* 13 (1978) 195.
4. K.L. Reifsnider and A.L. Highsmith, in *Composite Laminate Materials: Experimental and Design in Fatigue*, Westbury House, Guildford, England (1981).
5. A.L. Highsmith nad K.L. Reifsnider, in *Damage in Composite Materials*, ASTM STP 775 (1982) 103.
6. F.W. Crossman and A.S.D. Wang, in *Damage in Composite Materials*, ASTM STP 775 (1982) 118.
7. A.S.D. Wang and F.W. Crossman, *Journal of Composite Materials, Supplement* 14(1) (1980) 71.
8. F.W. Crossman, WT. Warren, A.S.D. Wang and G.E. Law, *Journal of Composite Materials, Supplement* 14(1) (1980) 88.
9. A.S.D. Wang, N.N. Kishore and C.A. Li, *Composite Science Technology* 24 (1985) 1.

10. G.P. Sendeckyj and W.F. Jones, *Engineering Fracture Mechanics* (in press).
11. W.F. Jones, "On the Accuracy of Higher Order Shear Lag Models," Engineering Science Preprint ESP22/85046, Society of Engineering Science, October 1985.
12. J.M. Hedgepeth, *Stress Concentration in Filamentary Structures*, NASA TN D-882 (1961).
13. J.G. Goree and R.S. Gross, *Engineering Fracture Mechanics* 13 (1979) 563.
14. J.A. Nairn, *Journal of Composite Materials* 22 (1988) 561–588.
15. R.M. Jones, *Mechanics of Composite Materials*, McGraw-Hill Book Company (1975).
16. R.J. Nuismer and J.M. Whitney, *Fracture Mechanics of Composites*, ASTM STP 593 (1975) 117–142.
17. L.R. Dharani, W.F. Jones and J.G. Goree, *Engineering Fracture Mechanics* 17 (1983) 555–573.